Nonlinear Evolution of the Lower-Hybrid Drift Instability in a Current Sheet

William Daughton,[1] Giovanni Lapenta,[1,2] and Paolo Ricci[1,2]
[1]*Los Alamos National Laboratory, Los Alamos, New Mexico 87545, USA*
[2]*Istituto Nazionale per la Fisica della Materia (INFM), Sezione di Torino, Italy*
(Received 2 April 2004; published 2 September 2004)

The lower-hybrid drift instability is simulated in an ion-scale current sheet using a fully kinetic approach with values of the ion to electron mass ratio up to $m_i/m_e = 1836$. Although the instability is localized on the edge of the layer, the nonlinear development increases the electron flow velocity in the central region resulting in a strong bifurcation of the current density and significant anisotropic heating of the electrons. This dramatically enhances the collisionless tearing mode and may lead to the rapid onset of magnetic reconnection for current sheets near the critical scale.

DOI: 10.1103/PhysRevLett.93.105004 PACS numbers: 52.35.Vd, 52.35.Kt, 94.30.Ej, 94.30.Gm

Current sheets with characteristic thickness of the order of a thermal ion gyroradius ρ_i are routinely observed in Earth's magnetosphere [1,2] and within laboratory experiments designed to examine the physics of magnetic reconnection [3], a topic with widespread application to space, astrophysical, and laboratory plasmas. Although current sheets are unstable to a variety of plasma instabilities including collisionless tearing [4] and the lower-hybrid drift instability [5], the relative importance of these instabilities to the onset and development of large scale magnetic reconnection remains controversial.

The lower-hybrid drift instability (LHDI) is driven by the diamagnetic current in the presence of inhomogeneities in the density and magnetic field [6]. The LHDI has been considered extensively as a possible candidate to modify the reconnection physics through anomalous resistivity generated by wave particle interactions [5,7,8]. Unfortunately, theory predicts the fastest growing modes with a wavelength on the electron gyroscale $k_y\rho_e \sim 1$ are localized on the edge of the layer [5], while enhanced fluctuations are required in the central region to produce significant anomalous resistivity. This conclusion is supported by observations at the magnetopause [9], in the magnetotail [10], and by laboratory experiments [11].

Based on this evidence, some researchers have concluded the LHDI does not play an important role in current sheet dynamics. However, new results from both theory and simulation are beginning to challenge this conclusion. In a number of simulations, a strong enhancement of the central current density associated with the LHDI is observed [12–16] and it has been suggested this effect gives rise to the rapid onset of reconnection [14,15]. Most of these simulations were performed with artificial ion to electron mass ratios $m_i/m_e \approx 100$–400 and very thin layers $\rho_i/L \approx 1.7$–2.2, where L is the half thickness of the layer. Although the simulations in Ref. [13] considered thicker layers at realistic mass ratio, the focus was on long wavelength effects, and the spatial resolution was insufficient to resolve the full LHDI spectrum.

The very thin layers considered in most of the simulations are comparable in thickness to laboratory reconnection experiments [3,17] but are considerably thinner than observed in the magnetotail prior to onset. In this regime, kinetic simulations indicate significant penetration of electromagnetic fluctuations into the central region [7,8,12]. An explanation for these waves was recently proposed based on a new approach to the linear Vlasov stability [18], which predicts the longer wavelength LHDI with $k_y\sqrt{\rho_i\rho_e} \sim 1$ can penetrate into the central region even though the fastest growing modes with $k_y\rho_e \sim 1$ are confined to the edge. The required thickness for this penetration [18] is approximately $\rho_i/L \gtrsim 1.5$.

In the magnetotail, the observed thickness of the current sheet [1] is larger ($\rho_i/L \lesssim 1$) and it appears the LHDI is well localized on the edge. In this work, the nonlinear evolution of the LHDI is examined for this regime using a two-dimensional kinetic approach with the physical value of the mass ratio for a hydrogen plasma $m_i/m_e = 1836$ and fully resolving all relevant spatial and temporal scales. The nonlinear development leads to a rich variety of interesting new physics including a strong bifurcation of the current density and significant anisotropic heating of the electron distribution in the central region. Furthermore, a simple physics model is proposed which can explain both of these features. These new results may have direct relevance in understanding bifurcated current sheets recently observed in the magnetotail [19,20]. In addition, these modifications greatly enhance the collisionless tearing mode and may play a crucial role in determining the onset of reconnection [21].

The initial configuration is a Harris sheet [22] with magnetic field $B_x = B_o \tanh(z/L)$ and plasma current $J_y = J_o \mathrm{sech}^2(z/L)$. The initial distributions are drifting Maxwellians with thermal velocity $v_{th_s} \equiv (2T_s/m_s)^{1/2}$ and uniform drift $U_s = 2cT_s/(q_sB_oL)$ where T_s is the temperature, m_s is the mass, q_s is the charge, $n(z) \equiv n_o \mathrm{sech}^2(z/L)$ is the density profile, and $s = i, e$ for ions and electrons. A uniform background distribution at rest

is also included, since the stability properties are sensitive to this feature [18]. The equilibrium parameters are $\rho_i/L = 1$, $T_i/T_e = 5$, $\omega_{pe}/\Omega_{ce} = 4$, and $n_b/n_o = 0.02$, where $\rho_i = v_{th_i}/\Omega_{ci}$ is an ion gyroradius, $\Omega_{cs} = eB_o/(m_s c)$ is the gyrofrequency computed from the asymptotic field B_o, $\omega_{pe} = (4\pi n_o e^2/m_e)^{1/2}$ is the plasma frequency calculated from the peak density n_o, and n_b is the background density with temperature $T_b = T_e$. These parameters are roughly appropriate for conditions observed in the magnetotail [1,23]. Simulations were performed for two different mass ratios: $m_i/m_e = 1836$ to simulate realistic conditions over a short duration and $m_i/m_e = 512$ to examine the evolution over a longer period.

The simulations are based on an algorithm in which the fields are advanced using the scalar and vector potentials [24,25]. Working in the Coulomb gauge, the scalar potential is computed directly from Poisson's equation, while the vector potential is advanced in time using a semi-implicit method, which permits the time step to exceed the Courant limit [25]. For waves with phase velocity much less than the speed of light, this approach is very accurate and comparisons against a fully explicit method [24] have revealed no significant differences. The boundary conditions for the particles and fields are periodic in the y direction. Conducting boundary conditions are imposed for the fields at the z boundaries and particles are reflected. In both simulations, the box size is $12L \times 12L$ and the time step is $\Delta t \Omega_{ce} = 0.1$, which fully resolves the electron motion but is approximately 6 times faster than the Courant limit. For $m_i/m_e = 1836$, the spatial grid is 5120×5120 with 6×10^9 particles while for $m_i/m_e = 512$, the spatial grid is 2560×2560 with 1.6×10^9 particles. This corresponds to a cell size $\Delta \approx 1.3\Lambda_D$ where Λ_D is a Debye length.

At the physical mass ratio $m_i/m_e = 1836$, the fastest growing mode from a linear Vlasov calculation [18] has wavelength $k_y\rho_e \approx 0.5$ with real frequency $\omega/\Omega_{ci} \approx 27.9$, growth rate $\gamma/\Omega_{ci} \approx 5.7$, and is localized in the region $0.7 \lesssim |z/L| \lesssim 2$. These predictions are in excellent agreement with the simulation results and fluctuations are well confined to the edge. Since the LHDI is driven by the diamagnetic drifts, one would expect a reduction of the current density in the region of LHDI activity and this expectation is confirmed in Fig. 1(a). The surprising result is the pronounced off-axis current filaments near $z/L \approx 0.2$. The modified current profile is largely due to changes in the electron fluid velocity V_{ey} as shown in Fig. 1(b) while changes in the ion fluid velocity and density are relatively minor. In addition, the electrons are heated in the direction perpendicular to the magnetic field resulting in a non-Maxwellian distribution in the central region, which may be roughly characterized in terms of the electron anisotropy $T_{e\perp}/T_{e\parallel}$ as shown in Fig. 1(c). At first glance, these results are perplexing since there is no wave activity in the region

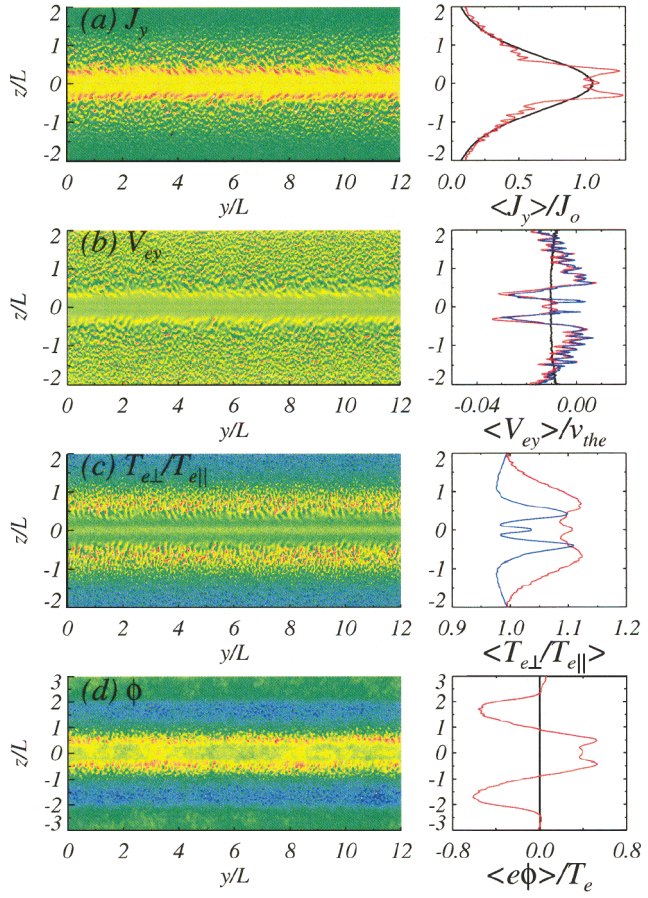

FIG. 1 (color). Simulation results for $m_i/m_e = 1836$ at time $t\Omega_{ci} = 7$ showing (a) current density J_y, (b) electron fluid velocity V_{ey}, (c) electron anisotropy $T_{e\perp}/T_{e\parallel}$, and (d) electrostatic potential ϕ. Contours of each quantity are shown on the left, while the y-average is shown on the right (red) along with the initial profile (black). The blue line in (b) corresponds to the y-average of the prediction for V_{ey} in Eq. (2), while the blue line in (c) corresponds to the anisotropy estimate in Eq. (3).

$|z/L| \lesssim 0.7$. Nevertheless, a simple physics model is sufficient to explain all of these results.

The constants of motion for a charged particle moving in the equilibrium field are $\varepsilon = m_s(v_z^2 + v_y^2)/2$, v_x, and $p_y = m_s v_y + q_s A_y/c$ where A_y is the vector potential $A_y = -B_o L \ln[\cosh(z/L)]$ for the Harris field. Particles with $\varepsilon > p_y^2/2m_s$ traverse both sides of the current layer and are referred to as *crossing* trajectories while particles with $\varepsilon < p_y^2/2m_s$ are confined to one side of the layer and are referred to as *noncrossing*. The boundary between crossing and noncrossing regions of phase space is

$$\frac{v_y}{v_{th_s}} = \frac{\alpha}{2} - \frac{1}{2\alpha}\left(\frac{v_z}{v_{th_s}}\right)^2, \tag{1}$$

where $\alpha = (L/\rho_s)\ln[\cosh(z/L)]$. An example cross section of phase space is illustrated in Fig. 2 for the region of the sheet with strong LHDI fluctuations. The parabolic curves correspond to Eq. (1) at the spatial positions $z/L = 1, 2$ while the concentric circles correspond to the

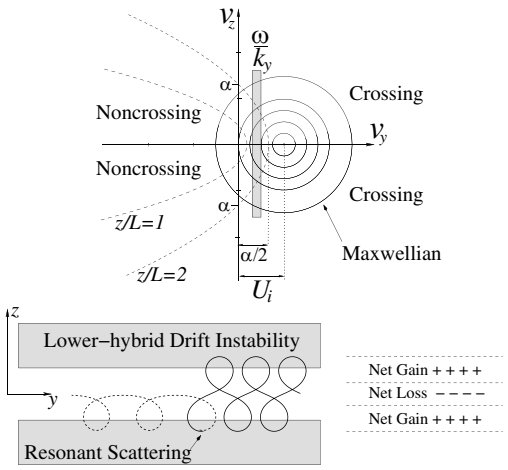

FIG. 2. Cross section of phase space (top) in the $v_z - v_y$ plane, illustrating a drifting Maxwellian ion distribution and the phase space boundary in Eq. (1) for two different spatial positions within the layer. The shaded region in the upper figure corresponds to the approximate phase velocity of the waves $\omega/k_y \approx U_i/2$, which are in the proper region to resonantly scatter crossing ions into the noncrossing region of phase space. This scattering process and the resulting charge accumulation is illustrated in the lower figure.

Maxwellian ion distribution. The phase space boundary is the only feature which varies with position in Fig. 2 since both the ion drift U_i and temperature T_i are spatially uniform. The approximate phase velocity for cold electrons $\omega/k_y \approx U_i/2$ is shown in the shaded region. The essential point is the phase velocity is in the proper region to permit a resonant scattering of ions from the crossing region into the noncrossing region as illustrated at the bottom of Fig. 2. Although the reverse scattering process is also possible, the slope of the distribution in the vicinity of the resonance favors the process shown in Fig. 2. This type of scattering can only occur if the spatial extent of the crossing ion orbits $\delta_i \approx \sqrt{2\rho_i L}$ overlaps with the spatial localization of the mode. It has been suggested that this process may lead to the creation of significant shear in the ion velocity [26]. In the present context, the resonant scattering leads to a loss of positive charge in the center in conjunction with a gain in the edge region, and therefore gives rise to an electrostatic potential structure across the layer as shown in Fig. 1(d).

To understand the increase in the electron flow velocity, consider the electron momentum equation within the fluid approximation. Neglecting the inertia term and using the equilibrium distribution to evaluate the pressure tensor, the resulting electron flow velocity is

$$V_{ey} \approx \frac{U_e}{1 + (n_b/n_o)\cosh^2(z/L)} - \frac{c}{B_x}\frac{\partial \phi}{\partial z}. \qquad (2)$$

The first term is the equilibrium flow while the second term is the $\mathbf{E} \times \mathbf{B}$ drift induced by the electrostatic potential. At early times within the simulation, the electron velocity is in excellent agreement with Eq. (2) as shown in Fig. 1(b), indicating the acceleration is a direct result of the electrostatic potential. As the simulation proceeds, the electron pressure is strongly modified and the simple relationship in Eq. (2) is no longer accurate. The ion flow is also modified, but to a much smaller degree due to the large inertia. The essential physics of this electron acceleration process is very different from recent results [14,15] in which an inductive electric field plays the dominant role while the electrostatic field is negligible [14]. In addition, these low mass ratio simulations do not observe the strong current bifurcation. Although our simulations confirm the bifurcated current structure is diminished at lower mass ratio, the electrostatic potential continues to play an essential role in the electron acceleration.

The anisotropic electron heating in the outer region $|z/L| \gtrsim 0.7$ is a direct consequence of the LHDI due to the electron ∇B drift resonance [6]. In the central region there are no fluctuations and this mechanism is not relevant. A different approach to explain the heating is to examine the adiabatic invariants for the various electron orbits. For a system with periodic motion, the action integral taken over a period $\oint pdq$ is a constant of the motion, where p and q are the generalized momentum and coordinate describing the periodic motion. When a change is imposed on the system so that the motion is no longer exactly periodic, the integral $\oint pdq$ is an adiabatic invariant provided that the change is slow in comparison to the period of motion. For the case of noncrossing electrons with helical trajectories, the well-known magnetic moment $\mu \equiv m v_\perp^2/(2B_x)$ is the relevant adiabatic invariant. This implies the perpendicular temperature is simply related to the local magnetic field

$$\frac{T_{e\perp}(z,t)}{T_{e\perp}(z,t=0)} \approx \frac{B_x(z,t)}{B_x(z,t=0)}. \qquad (3)$$

For the region $0.3 \lesssim |z/L| \lesssim 0.5$ where the electron orbits are helical, this expression provides a good estimate of the perpendicular heating as shown by the blue line in Fig. 1(c). In the central region $|z/L| < 0.2$, the electron trajectories undergo a variety of complicated crossing orbits and μ is no longer the relevant invariant. Approaches for constructing adiabatic invariants in regions of strong gradients [27] will be examined in future work.

These results demonstrate the essential physics of the nonlinear deformation at early time for realistic mass ratio. This process leads to a significant increase in the electron velocity in the range $|z/L| \lesssim 0.5$ and since the LHDI is driven by the relative drift between electrons and ions, one would expect the spatial region of wave activity to move inward. This in turn would lead to more ion scattering and further enhancements to the electrostatic potential, current bifurcation, and electron anisotropy. Unfortunately, to confirm this scenario at realistic mass ratio is prohibitively expensive. However, longer simula-

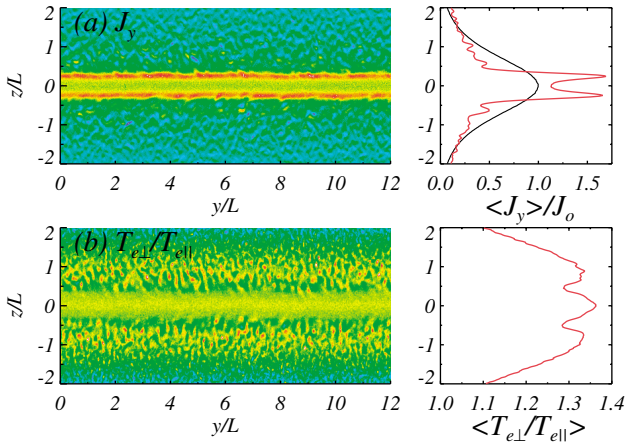

FIG. 3 (color). Late time evolution for $m_i/m_e = 512$ at $t\Omega_{ci} = 29$ showing (a) current density J_y and (b) electron anisotropy $T_{e\perp}/T_{e\|}$. The y-averaged profiles (red) and initial current density (black) are shown on the right.

tions performed with the reduced mass ratio $m_i/m_e = 512$ confirm this hypothesis. As shown in Fig. 3 at time $t\Omega_{ci} = 29$, the peak current density increases by nearly 70% while the electron anisotropy reaches $T_{e\perp}/T_{e\|} \approx 1.35$ in the central region. At earlier time $t\Omega_{ci} = 7$, the anisotropy in the central region $T_{e\perp}/T_{e\|} \approx 1.12$ is only slightly larger than the $m_i/m_e = 1836$ result in Fig. 1(c). These relatively small changes to the electron distribution can be difficult to compute accurately in explicit particle-in-cell simulation due to the issue of numerical electron heating. To check the sensitivity, the $m_i/m_e = 512$ simulation was repeated with 3 times as many particles (5×10^9) and a smaller time step $\Delta t\Omega_{ce} = 0.075$. The resulting electron anisotropy at time $t\Omega_{ci} = 7$ is only slightly smaller ($T_{e\perp}/T_{e\|} \approx 1.09$) indicating numerical heating is relatively minor.

In summary, the LHDI has been simulated for the first time at physically realistic mass ratio using a fully kinetic approach, which resolves all relevant scales. For the initial sheet thickness $\rho_i/L = 1$, the modes are localized on the edge of the layer in agreement with linear theory. Nevertheless, the nonlinear evolution gives rise to a resonant scattering of crossing ions into the noncrossing region of phase space. This in turn produces an electrostatic potential structure across the sheet leading to a strong bifurcation of the current density and perpendicular electron heating. The collisionless tearing mode is driven by the gradient of the current density [4], but is also very sensitive to the electron anisotropy [28,29]. Thus the nonlinear development of the LHDI can dramatically increase the growth rate of tearing without invoking anomalous resistivity. For the $m_i/m_e = 1836$ case in this Letter, the maximum tearing growth rate with isotropic electrons is $\gamma/\Omega_{ci} \approx 0.035$ at $k_x L \approx 0.45$, while for $T_{e\perp}/T_{e\|} \approx 1.1$ this increases to $\gamma/\Omega_{ci} \approx 2.2$ with $k_x L \approx 4$. Simulations indicate the rapid growth and coalescence of these small scale tearing islands can result in the onset of large scale reconnection [21]. This mechanism is activated when the current layer approaches a critical thickness $\rho_i/L \approx 0.5$ where the crossing ion trajectories extend into the spatial region of LHDI activity.

This work was supported by the LDRD program at Los Alamos National Laboratory and by NASA Geospace Sciences. The authors gratefully acknowledge useful discussions with J. Brackbill, D. Winske, and P. Pritchett.

[1] V. A. Sergeev, D. G. Mitchell, C. T. Russell, and D. J. Williams, J. Geophys. Res. **98**, 17 345 (1993).
[2] V. A. Sergeev, V. Angelopoulos, C. Carlson, and P. Stutcliffe, J. Geophys. Res. **103**, 9177 (1998).
[3] M. Yamada, H. Ji, S. Hsu, T. Carter, R. Kulsrud, and F. Trintchouk, Phys. Plasmas **7**, 1781 (2000).
[4] B. Coppi, G. Laval, and R. Pellat, Phys. Rev. Lett. **16**, 1207 (1966).
[5] J. D. Huba, J. F. Drake, and N. T. Gladd, Phys. Fluids **23**, 552 (1980).
[6] R. C. Davidson, N. T. Gladd, C. S. Wu, and J. D. Huba, Phys. Fluids **20**, 301 (1977).
[7] D. Winske, Phys. Fluids **24**, 1069 (1981).
[8] M. Tanaka and T. Sato, J. Geophys. Res. **86**, 5541 (1981).
[9] S. D. Bale, F. S. Mozer, and T. Phan, Geophys. Res. Lett. **29**, 2180 (2002).
[10] I. Shinohara, T. Nagai, M. Fujimoto, T. Terasawa *et al.*, J. Geophys. Res. **103**, 20 365 (1998).
[11] T. Carter, H. Ji, F. Trintchouk, M. Yamada, and R. Kulsrud, Phys. Rev. Lett. **88**, 015001 (2002).
[12] R. Horiuchi and T. Sato, Phys. Plasmas **6**, 4565 (1999).
[13] G. Lapenta and J. U. Brackbill, Phys. Plasmas **9**, 1544 (2002).
[14] M. Scholer, I. Sidorenko, C. Jaroscheck, R. Treumann, and A. Zeiler, Phys. Plasmas **10**, 3521 (2003).
[15] I. Shinohara and M. Fujimoto (to be published).
[16] P. Pritchett, in *Proceedings of the ICS-6*, edited by R. Winglee (University of Washington, Seattle, 2002), p. 225.
[17] H. Ji, S. Terry, M. Yamada, R. Kulsrud, A. Kuritsyn, and Y. Ren, Phys. Rev. Lett. **92**, 115001 (2004).
[18] W. Daughton, Phys. Plasmas **10**, 3103 (2003).
[19] A. Runov, R. Nakamura, W. Baumjohann *et al.*, Geophys. Res. Lett. **30**, 1036 (2003).
[20] V. A. Sergeev, A. Runov, W. Baumjohann *et al.*, Geophys. Res. Lett. **30**, 1327 (2003).
[21] P. Ricci, J. U. Brackbill, W. Daughton, and G. Lapenta, Phys. Plasmas **11**, 4489 2004.
[22] E. G. Harris, Nuovo Cimento **23**, 115 (1962).
[23] A. Lui, in *Magnetotail Physics*, edited by A. Lui (John Hopkins University Press, Baltimore, 1987), p.3.
[24] R. Morse and C. Nielson, Phys. Fluids **14**, 830 (1971).
[25] D. Forslund, in *Space Plasma Simulations*, edited by M. Ashour-Abdalla and D. Dutton (Reidel, Norwell, Massachusetts, 1985), p. 425.
[26] W. Daughton, Phys. Plasmas **9**, 3668 (2002).
[27] E. Whipple, J. Geophys. Res. **91**, 4149 (1986).
[28] D. Forslund, Ph.D., thesis, Princeton University, 1968.
[29] J. Chen and P. Palmadesso, Phys. Fluids **27**, 1198 (1984).